Helmholtz-Zentrum Dresden-Rossendorf (HZDR)

HELMHOLTZ ZENTRUM
DRESDEN ROSSENDORF

Probing the local coordination of hexavalent uranium and the splitting of 5f orbitals induced by chemical bonding.

Amidani, L.; Retegan, M.; Volkova, A.; Popa, K.; Martin, P. M.; Kvashnina, K.;

Originally published:

October 2021

Analytical Chemistry 60(2021)21, 16286-16293

DOI: https://doi.org/10.1021/acs.inorgchem.1c02107

Perma-Link to Publication Repository of HZDR:

https://www.hzdr.de/publications/Publ-32849

Release of the secondary publication
on the basis of the German Copyright Law § 38 Section 4.

Probing the local coordination of hexavalent uranium and the splitting of 5f orbitals induced by chemical bonding.

Lucia Amidani,[1,2]* Marius Retegan,[3] Anna Volkova,[4] Karin Popa,[5] Philippe M. Martin,[6] Kristina O. Kvashnina[1,2,4]*

[1] The Rossendorf Beamline at ESRF, The European Synchrotron, CS40220, 38043 Grenoble Cedex 9, France.

[2] Institute of Resource Ecology, Helmholtz Zentrum Dresden-Rossendorf (HZDR), PO Box 510119, 01314 Dresden.

[3] ESRF – The European Synchrotron, CS40220, 38043 Grenoble Cedex 9, France.

[4] Lomonosov Moscow State University, Department of Chemistry, 119991 Moscow, Russia.

[5] European Commission, Joint Research Centre, Nuclear Safety and Security Directorate, P.O. Box 2340, 76125 Karlsruhe, Germany.

[6] CEA, DES, ISEC, DMRC, University of Montpellier, Marcoule, France.

ABSTRACT: We report here the first detailed experimental and theoretical investigation of hexavalent uranium in various local configurations with high-energy-resolution fluorescence-detected X-ray absorption near-edge structure at the M_4 edge. We demonstrate the pronounced sensitivity of the technique to the arrangement of atoms around the absorber and provide a detailed theoretical interpretation revealing the nature of spectral features. We show that for all local configuration analyzed, the main peak corresponds to non-bonding 5f orbitals, and the highest energy peak corresponds to anti-bonding 5f orbitals. Our findings are in agreement with the accepted interpretation of uranyl spectral features and embed the latter in the broader field of view where the spectra of a larger variety of U^{6+}-containing samples are interpreted on the same theoretical ground.

Introduction

In the investigation of actinide-based compounds, the application of $M_{4,5}$ edges X-ray Absorption Near-Edge Structure (XANES) in the High-Energy-Resolution Fluorescence-Detected (HERFD) mode is acquiring increasing popularity [1–12]. By probing the 5f electronic structure directly, this technique is very appealing to investigate fundamental properties of actinides, whose knowledge lags behind that of more stable elements. The progressive filling of the 5f electronic shell along the actinide series is at the base of the fascinating variety of actinide chemistry. Different from the 4f shell, which due to the screening of outer-lying occupied shells is almost core-like and weakly influenced by the atomic surrounding, the 5f shell extends out from the atomic core in the valence region. It is consequently more prone to participate to bonds.[13] As a result, the first half of the actinide series exhibits many stable oxidation states and a great variety of local coordination geometries compared to lanthanides.[14] Determining the 5f shell occupancy and the degree of its involvement in bonds is fundamental to understand and control actinides chemistry.

In this respect, a central role is played by $M_{4,5}$ edges HERFD XANES, a powerful tool to interrogate actinide 5f electronic structure directly. Their sensitivity to the oxidation state is well established and strongly founded on the comparison with references of well-known valence and calculations taking into account electron-electron correlations.[1,15,16] Conversely, extracting information on the local environment and the covalency of bonds is less obvious. Performing theoretical calculations that reproduce the observed experimental data is often necessary to have an insight into these properties. Calculating the $M_{4,5}$ HERFD XANES of actinides is particularly challenging, since electrostatic interactions, spin-orbit coupling, and interaction with ligands are all relevant for the 5f states. As the former are the strongest interactions, the appropriate theoretical approaches are the atomic multiplet theory or more sophisticated methods that can treat multi-electronic effects.[15–18] At the same time, actinides chemistry comprises cases of great relevance where the 5f shell is empty or singly occupied, the most prominent example being U^{6+}. These simpler cases can elucidate the sensitivity of $M_{4,5}$ spectral shape to local environment and bond covalency by Density Functional Theory (DFT) based methods, which naturally account for the local environment and calculate the electron density involved in bonds.

In this work, we report an in-depth study of M_4 edge HERFD XANES spectra of four U^{6+} compounds where U local coordination varies from almost perfect octahedral (O_h), i.e., uranate, to compressed octahedral (D_{4h}) and distorted hexagonal bipyramid (D_{3d}) presenting shorter U – O bonds similar to the trans-dioxo uranyl ion. Experimental HERFD XANES exhibit marked differences that can be well reproduced with DFT-based XANES calculations. Inspection of the underlying U f-density of states (DOS) guides the assignment of spectral features to specific f-orbitals and provides insight into the bonding with neighbouring ligands.[19] We have compared the DFT results with crystal field multiplet theory calculations using various point group symmetries and the interpretation of spectral features is confirmed.

Altogether, the present work is a comprehensive study on the dependence of U^{6+} M_4 HERFD XANES spectra on local coordination in a variety of local symmetries. A unified picture emerges on the high sensitivity of this technique in probing the splitting of 5f orbitals induced by the specific arrangement of ligands. The possibility to accurately reproduce

with DFT calculations the trends correlated to local coordination offers a powerful tool for U $M_{4,5}$ HERFD XANES analysis, which can be extended to actinides with empty and singly occupied 5f-shell.

Experimental and Computational details

Details on sample preparation and characterization can be found in ref. 20 for $CaUO_4$, Sr_3UO_6 and $SrUO_4$ and ref. 21 for $Cs_2UO_2Cl_4$. XRD showed that each compound was single phase and well crystallized.

For X-ray measurements, few mg of sample powder were mixed with boron nitride and pressed as a pellet. M_4 edge HERFD XANES spectra were collected at the beamline ID26 of the European Synchrotron Radiation Facility (ESRF).[22] The incident beam energy was selected by a Si(111) double crystal monochromator. Rejection of higher harmonics was achieved by three Si mirrors at an angle of 3.5 mrad relative to the incident beam. XANES spectra were measured in HERFD mode by recording the intensity at the maximum of the U M_β emission line (3336.0 eV) as a function of the incident energy. The emission energy was selected by an X-ray emission spectrometer equipped with five spherically bent Si(222) crystal analysers. All spectra were acquired at the same time except $Cs_2UO_2Cl_4$, measured in a different experimental session. The latter was aligned to the other samples based on references common to both experiments.

FDMNES calculations[23,24] of the U M_4 edge XANES were performed with the Finite Difference Method (FDM), considering a cluster of 6.0 Å around the absorber. Within this cluster, the atomic potential was calculated self-consistently. Atomic coordinates were taken from structural data deposited in the International Crystal Structure Database (ICDS).[25] Scalar relativistic and spin-orbit effects were included and the impact of the core-hole on the spectral shape evaluated with the help of the screening parameter. Projected DOS were calculated together with XANES spectra. When required, the atomic coordinates of the clusters around the absorber were rotated to have the U – O short bonds along the z-axis and the basis-set correctly oriented with respect to the local symmetry. The convolution parameters were set to reproduce the sharpening obtained with HERFD mode (*Gamma_hole* = 0.2 eV, *Gamma_max* = 0.5 eV). An example of FDMNES input file is provided in the Supplementary Information (SI).

Crystal field multiplet (CFM) calculations for U^{6+} in O_h and D_{4h} symmetry were performed with the code Quanty,[26] using the input file generated with Crispy interface.[27] The crystal field strength was tuned by setting directly the energies of the 5f orbitals belonging to the different irreducible representation. The CF parameters and the Slater-Condon integrals for the initial and final states were kept the same. The strength of the integrals was set to 0.4 after testing values between 0.8 and zero. The inclusion of hybridization was tested and strong correlation between CF and hybridization parameters was found. Since a unique set of parameters for CF and hybridization could not be determined, results including only CF are presented. CFM calculations were convoluted with a Lorentzian and a Gaussian function, with a FWHM of 0.5 eV. An example of input file is provided as SI.

Results and Discussion

Hexavalent uranium (U^{6+}) plays a crucial role in actinide chemistry. The hexavalent is the most frequent state of uranium in solution and the solid-state as it is the most stable oxidation state adopted by uranium. Its speciation and chemistry are fundamental for uranium-based nuclear fuels, safe nuclear waste disposal, and radionuclides diffusion in the environment. In solution, U^{6+} is found in the trans-dioxo uranyl moiety, forming ultra-short linear bonds with two oxygen atoms. When incorporated in the solid-state, it exhibits a great flexibility of bonding, giving rise to an extremely rich structural topology that has been thoroughly investigated in the works by Burns and collaborators.[14,28] When bound to 7 or 8 ligands, U^{6+} is always found as uranyl. However, the arrangement of the rest of the ligands, the length of bonds, and the linearity of the uranyl unit can vary significantly. When surrounded by 6 anions, U^{6+} can assume an almost regular octahedral configuration, referred to as uranate, or a compressed octahedral symmetry with two shorter and 4 longer bonds. More rarely, it can also be found in a sort of anti-uranyl configuration, with 4 shorter and 2 longer bonds.[29]

The four compounds investigated in this work are Sr_3UO_6, $CaUO_4$, β-$SrUO_4$, and $Cs_2UO_2Cl_4$ and are representative of the diversity of local coordination assumed by hexavalent uranium. The unit cells, the local coordination of U^{6+} and the nearest neighbour distances are shown in Figure 1. From left to right, the structures are ordered according to the decrease of the shortest U – O bonds. In Sr_3UO_6 uranate, U^{6+} is in almost perfect octahedral symmetry, with only 0.034 Å maximum difference between U – O bonds. In $CaUO_4$, U^{6+} is surrounded by 2 O atoms, forming short and linear U – O bonds (1.961 Å) and 6 O atoms at longer distance (2.295 Å) uniformly distributed around the equatorial plane. More precisely, they are alternatively scattered off the equatorial plane by ±13°, giving a D_{3d} local symmetry. The difference between longest – shortest U – O bonds is 0.33 Å, ten times larger than in uranate. In β-$SrUO_4$, U is at the centre of a compressed square bipyramids with 2 shorter apical (1.877 Å) and 4 longer equatorial (2.186 – 2.205 Å) bonds in D_{4h} local symmetry. The maximum difference in bond length is 0.33 Å. U^{6+} in $Cs_2UO_2Cl_4$ is also in D_{4h} local symmetry, with two shorter U – O bonds (1.78 Å) and 4 longer U – Cl bonds (2.665 – 2.687 Å) on the equatorial plane. The difference between long and short bonds is 0.9 Å. Following the classification of Burns et al.,[14] reporting 1.816 Å as the average uranyl bond length in U^{6+} compounds with 6 ligands, $Cs_2UO_2Cl_4$ contains uranyl, β-$SrUO_4$ is intermediate between uranyl and uranate and Sr_3UO_6 is holosymmetric. $CaUO_4$, similarly to β-$SrUO_4$, represents an intermediate case.

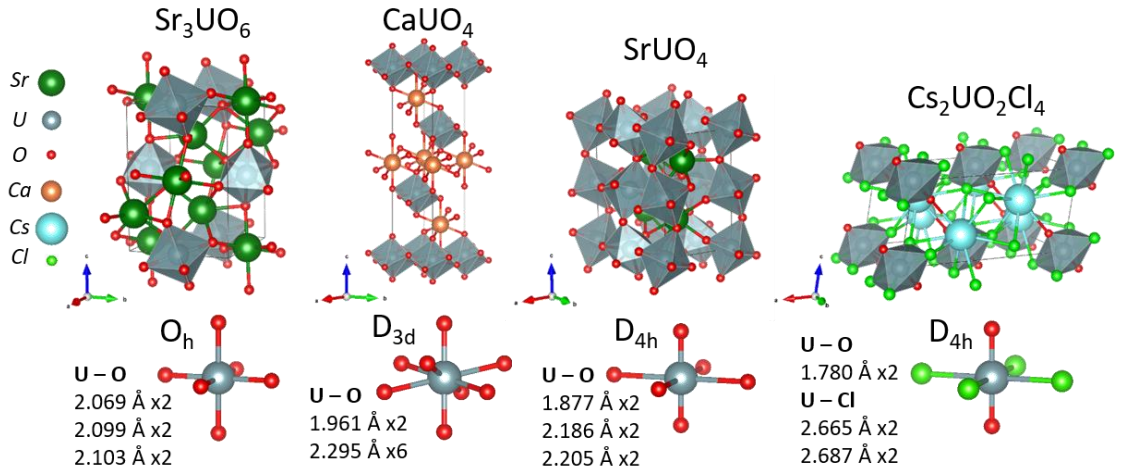

Figure 1: Unit cell (top) and local coordination of U and bond distances (bottom) for the set of compounds under study.

The topology of U polyhedra in the set of compounds is also different. β-$SrUO_4$ and $CaUO_4$ exhibit layers of polyhedra intercalated by alkaline ions. Sr_3UO_6 and $Cs_2UO_2Cl_4$ are among the rare compounds where polyhedra are isolated.[14]

U M_4 HERFD XANES spectra of the four compounds are shown in Figure 2 (thick lines). Calculated XANES (thin lines) and f-DOS (dotted lines) obtained by FDMNES are also shown and will be discussed in the following. A first examination of the spectra indicates that significant differences modulate a somewhat similar spectral shape. All spectra present a sharp rise of the absorption at the same energy, followed by a steep decrease of intensity intercalated by spectral features and terminating with a low-intensity peak. The energy separation between the first and the last peak and the number of features in between are system-dependent. In Sr_3UO_6 and $Cs_2UO_2Cl_4$, three peaks are well distinguished and labelled A, B and C. In β-$SrUO_4$ and $CaUO_4$, only A and C can be identified, with β-$SrUO_4$ presenting two shoulders in between while no additional feature is distinguished for $CaUO_4$.

The most striking difference is the increased energy of peaks C, which shifts of 3.6 eV going from Sr_3UO_6 to $Cs_2UO_2Cl_4$. Spectra are ordered from top to bottom according to decreasing length of the shortest U – O bond, suggesting that the energy of peak C might correlate with it. This correlation is indeed well-established in the case of uranyl compounds, represented here by $Cs_2UO_2Cl_4$. In an early publication showing conventional U M_5 XANES of uranyl, peaks B and C were assigned to the fπ* and fσ* anti-bonding molecular orbitals of the $U–O_{yl}$ moiety.[4] This assignment was then confirmed and put on solid ground by polarization dependent HERFD XANES at U M_4 edge supported by molecular orbital calculations on $Cs_2UO_2Cl_4$.[21] Many subsequent works using U M_4 HERFD XANES and EXAFS data confirmed the correlation between the length of the uranyl bond and the position of peak C.[9,30,31] A shift of C to lower energy was observed upon dehydration of studtite and associated to the elongation of the $U–O_{yl}$ bonds and DFT-based calculations supported the results.[31] Uranyl compounds have been frequently studied with $M_{4,5}$ HERFD XANES and uranyl spectral shape, characterized by three well-separated peaks, is well-known and exploited to detect its presence. On the contrary, $M_{4,5}$ HERFD XANES investigations on hexavalent uranium in other local configurations are rare[32] and this is the first work reporting a direct comparison of U^{6+} in different local configurations. A important remark is that the three peaks are also characteristic of uranate and that more than three structures may be observed in systems with very short U–O bonds similar to uranyl.

To prove the sensitivity of $M_{4,5}$ HERFD XANES to the local coordination environment, we performed FDMNES calculations starting from the crystal structures of the four compounds. The results are reported in Figure 2, where calculated spectra have been aligned experimental data. The agreement is remarkably good, and all major features are reproduced by the calculations. In particular, the shift of the

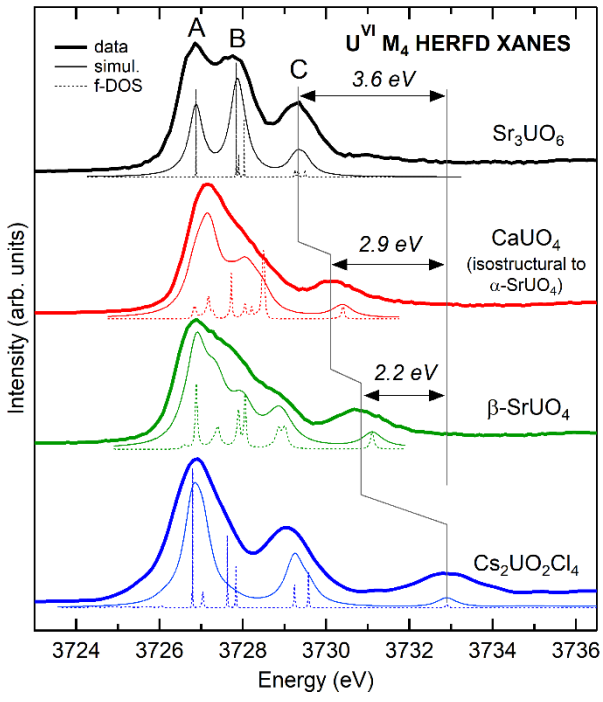

Figure 2: Experimental (thick line) and simulated (thin line) U M_4 HERFD XANES for all samples. The corresponding U f-DOS are reported below each simulation (dotted line). The shifts of peak C along the set are reported highlighted by a vertical line.

peaks C and the different number of structures observed in between. The relative position of A and C is rather well reproduced for all compounds. Three peaks at the correct energy are simulated for Sr_3UO_6 and $Cs_2UO_2Cl_4$. A single structure is observed in the simulation of $CaUO_4$ between peak A and C, while multiple shoulders are predicted for β-$SrUO_4$ in good agreement with experimental data. The fact that the main trends observed experimentally, i.e., number, position, and relative intensities of features, are reproduced by calculations confirms that the different local environment are responsible for the variations observed. Inspection of each simulated compound reveals however minor discrepancies, mostly related to the intensity of peaks. The intensity of peak A in Sr_3UO_6 uranate is underestimated. In the experimental data of $CaUO_4$, the spectrum is steeply decreasing after peak A, while a structure can be distinguished in the simulation. The position of the shoulders in β-$SrUO_4$ is not perfectly matching experimental data and, finally, the asymmetry of peak A in $Cs_2UO_2Cl_4$, which has a shoulder on the high-energy side, is not well reproduced. These differences may be ascribed to two main causes. The discrepancies mentioned for $CaUO_4$ and $Cs_2UO_2Cl_4$ are compatible with an incorrect selection of the f-DOS participating to the XANES, as suggested by the presence of peaks in the f-DOS of $Cs_2UO_2Cl_4$ in correspondence of the missing shoulder (Figure 2 and Figure S1). We recall that due to selection rules, the M_4 edge probes only partially the f-DOS, i.e., the $5f_{5/2}$ contribution. A similar discrepancy between FDMNES calculations and data has been observed by the authors at the M_4 edge of ThO_2.[33] The second source of discrepancies can be the real local structure of U compared to the average structure represented by the crystal structure. Indeed, EXAFS showed that the first U–O distance is slightly shorter compared to the value from PXRD results (2.04 Å instead of 2.07 Å)[20] and the intensity of the first peak in the XANES simulation increases if the local structure is modified according to EXAFS results. The improved spectrum is shown in Figure S2.

The f-DOS allows ascribing spectral features to specific f-orbitals and compares FDMNES results with the splitting expected from the local symmetry. Figure 3 reports the splitting of f-orbitals under O_h and D_{4h} symmetry. In O_h symmetry, the f-orbitals split in three irreducible representations. The t_{1u} group is the highest in energy and comprises three orbitals f_{x3}, f_{y3} and f_{z3} directed towards the ligands, placed at the centre of the face of a cube surrounding U. The a_{2u} irreducible representation comprises only the f_{xyz} orbital whose lobes points to the corner of the cube.[34] In D_{4h} symmetry, f-orbitals split in 5 groups. The energy of the f_{z3} orbital, now a_{2u}, is raised due to the shortening of bonds along the z-axis and becomes the highest in energy. The f_{xyz} orbital, now b_{1u}, remains the orbital with the weakest superposition with ligands and is still expected to be the lowest in energy. Figure 3 shows the f-DOS calculated for Sr_3UO_6 uranate (O_h) and $Cs_2UO_2Cl_4$ uranyl (D_{4h}) for the final calculations, using a fully screened and a partially screened (*Screening* = 0.6) core-hole (CH), respectively. To assign the spectral features to pure f-orbitals and highlight the effect of the CH, the U f-DOS is calculated in the absence of spin-orbit coupling and CH potential. Inclusion of the CH increases the relative separation of peaks and modulates their intensities. We notice that the f-DOS

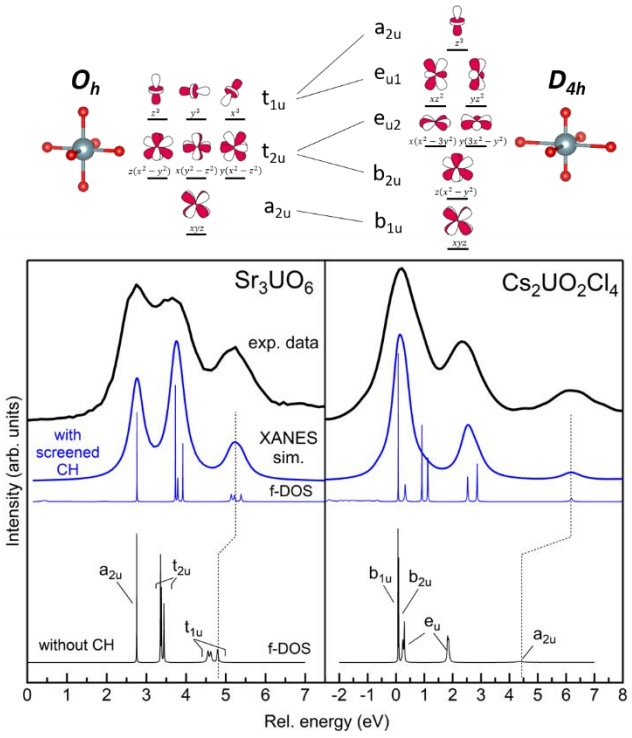

Figure 3: Top: Scheme of the splitting of f-orbitals under O_h (cubic set) and D_{4h} (general set) symmetry. Bottom: experimental data (top - black line) of Sr_3UO_6 and $Cs_2UO_2Cl_4$ are compared with XANES calculations obtained in the presence of a screened core-hole (blue thick line) and the corresponding U f-DOS (blue thin line). To assign feature to symmetry split orbitals and highlight the effect of the CH, the U f-DOS in the absence of spin-orbit and CH is shown on the bottom (thin black line). The vertical dotted line marks the shift of the higher energy peak.

has three groups of very sharp peaks that can be assigned to the splitting of the f-orbitals in O_h and D_{4h} symmetries, as indicated by labels in Fig. 3. The order in energy agrees with geometrical considerations. Peaks A, B, and C of Sr_3UO_6 uranate are assigned to a_{2u}, t_{2u} and t_{1u} orbitals. Peak A reflects therefore a single f-orbital, f_{xyz}, while two groups of three orbitals are beneath features B and C. Interestingly, below peak C, the three orbitals are slightly split, reflecting the different distances of O atoms (0.034 Å) from the central U. Indeed, this splitting causes the asymmetry of peak C observed in experimental data. In contrast, a more symmetric peak C is expected for a regular UO_6 octahedron. The asymmetry is well reproduced by utilizing U–O distances from EXAFS (Figure S2). In $Cs_2UO_2Cl_4$ several f-orbitals are found below peak A, i.e., b_{1u}, b_{2u} and one e_u. In the final simulation they split in two groups, in agreement with the observed asymmetry of peak A. However, the XANES calculation underestimate the intensity of the second group and the shoulder observed experimentally is not well reproduced. Peak B corresponds to the second e_u orbital group (f_{xz2} and f_{yz2}), and peak C to a_{2u} (f_{z3}). These f-orbitals are the same as the fπ* and fσ* anti-bonding molecular orbitals of the uranyl ion.[4,31,35] Our results further confirms previous assignments. Interestingly, the CH effect is fundamental to obtain good agreement in the relative energy position of peaks. Previous calculations based on molecular orbitals or DFT

indeed underestimated the separation between A and C, probably because of the absence of the CH effect.[21,31]

XANES calculations and corresponding f-DOS for the full set of compounds are reported in Figure S1. It is interesting to notice that $CaUO_4$ and β-$SrUO_4$ are better reproduce when the CH effect is neglected, and calculations reported in Figure 2 correspond to the case where the CH is not included (middle curves Fig. S1). Indeed, the CH has a remarkable effect on peak intensities and results in poor agreement with the experimental data. This fact suggests that the CH is better screened in these systems compared to Sr_3UO_6 uranate and $Cs_2UO_2Cl_4$ uranyl, a difference that may correlate with the topology of the samples, since the effect of the CH is more (less) pronounced for samples where U polyhedra are isolated (connected in corner-sharing sheets). This may indicate that after the creation of the CH, the U polyhedra neighbouring the absorber may furnish additional charge for screening. Figure S1 also reports the f-orbital contributions. The scheme with the f-orbital splitting in the D_{3d} symmetry is reported in Figure S3. Overall the calculations reveal that peak C always corresponds to the f_{z3} orbital, which points towards the ligands. Peak A corresponds to the orbitals less involved in bonding, purely non-bonding for the extreme cases of Sr_3UO_6 and $Cs_2UO_2Cl_4$. For features in between A and C, consideration of the specific local environment is necessary. Comparison of β-$SrUO_4$ and $Cs_2UO_2Cl_4$ indicate that the highest energy shoulder of the former corresponds to peak B of the latter, while other shoulders of β-$SrUO_4$ are due to orbitals that are all gathered beneath peak A in $Cs_2UO_2Cl_4$. The spectral shape and the f-orbital distribution of $CaUO_4$ differ substantially from the other systems presented, reflecting the different arrangement of ligands around the uranyl unit. Overall, the analysis of the spectra using the f-DOS allows precise assignment of spectral features and discloses similarities and differences stemming from the different local configurations. Most importantly, the capability to reproduce with calculations the spectral shape of such a variety of systems opens the door to the use of M_4 edge HERFD for more precise structural evaluation of U^{6+} bearing systems.

The numerous investigations on uranyl systems with $M_{4,5}$ HERFD XANES reveal a tight correlation between the separation of peak A and C, the length and covalency of the U–O_{yl} bond.[6,30] Our results demonstrate that two peaks originate from the same 5f orbitals and have similar bonding characteristics, i.e. anti-bonding for C and non-bonding for A. To verify a possible correlation over a larger class of cases, we report in Figure 4 the energy separation of two peaks as a function of the U–O bond length from several published data on uranyl compounds and the four systems investigated in this work. The dotted line is the linear fit of only uranyl samples, i.e., with bond length below 1.8 Å. We notice that the linear correlation intercepts only the uranyl compounds, while the rest of compounds deviate significantly from the fit. We notice that a more substantial effect of the core-hole potential for $CaUO_4$ and β-$SrUO_4$ would increase the A–C distance and push the corresponding points up and far away from the fit. The A–C peaks separation is therefore not a universal parameter correlated to U–O bond distance but may still furnish quantitative information on uranyl

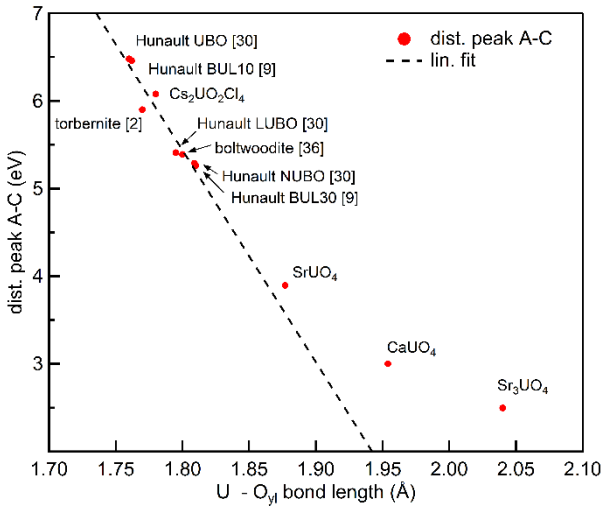

Figure 4: Distance between peak A and C of U M_4 edge HERFD versus U – O_{yl} bond length from [2,9,30,36] and the present data. The dashed line is the linear fit obtained considering uranyl samples, i.e., with U – O_{yl} bond length < 1.8 Å.

systems. The possibility to theoretically simulate the full spectrum remains the best tool to investigate the character of the bonds through a detailed analysis of the underlying f-DOS.

Similar agreement between DFT-based calculations and $M_{4,5}$ HERFD XANES is expected for actinides with empty or singly-occupied 5f shell were effects of electron correlations are expected to be minor. However, the increasing strength of multi-electronic interactions with the filling of the 5f shell demands alternative theoretical approaches. To our knowledge, works using sophisticated *ab initio* methods beyond DFT to simulate $M_{4,5}$ edges are still rare[17,18,37] and do not always brings satisfactory agreement with data. Semi-empirical multiplet theory is extensively used to account for multi-electronic interactions in X-ray spectroscopies.[2,38] Our samples require a few parameters to be simulated within the multiplet theory: the Slater-Condon (SC) integrals for the interaction between the 3d core-hole and the 5f photoexcited electron and the CF parameters. The strength of the CF parameters used in these cases can provide the starting point for systems with more 5f-electrons. We simulated the M_4 HERFD of U^{6+} for O_h and D_{4h} symmetries with the code Quanty and calculations giving the best agreement are reported in Figure 5 for Sr_3UO_6 (O_h), $SrUO_4$ (D_{4h}), and $Cs_2UO_2Cl_4$ (D_{4h}). The energies of the 5f-orbitals and the associated Wybourne CF parameters are reported in Table S1 and S2. In terms of the peaks positions the agreement with the experiment is reasonably good. The relative intensities are also in good agreement, with the exception of Sr_3UO_6 where the intensity of the first peak is significantly lower in calculations. This may reflect the deviation from the perfect O_h symmetry of the system, in line with the improvements in FDMNES calculations when EXAFS distances are considered. Interestingly, to obtain the correct relative intensity of spectral features, the Slater-Condon integrals were reduced to 40% of their atomic value. For the case of U^{6+} where the f-shell is empty, only the integrals between the 3d core-hole and the 5f photo-excited electron are non-zero. The need for such rather large reduction of the SC integrals can be explained by the strong involvement of U^{6+} 5f orbitals in covalent chemical bonds, in analogy with recent publications.[39,40]

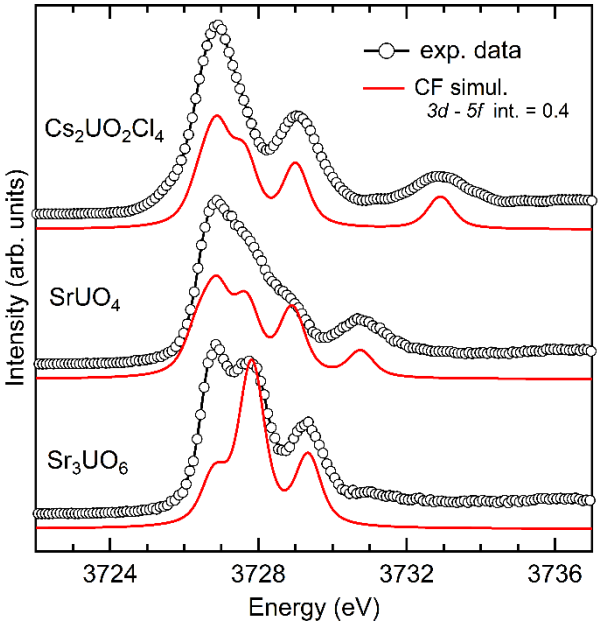

Figure 5: Comparison of experimental data (black open circles) and CFM calculations (red line) obtained with Slater-Condon integrals reduced at 40% of their atomic value.

Explicit treatment of covalency may lead to a more reasonable reduction factor, as show by Agrestini et al.[39]

To identify the origin of the spectral features in the calculations we have independently varied the energy of the 5f-orbitals corresponding to each irreducible representation. We shifted each group of orbitals by ±0.4 eV in steps of 0.2 eV. The results of this *in silico* exercise are shown in Figure 6, where smaller convolution parameters were adopted to better appreciate the shift of spectral features. The results nicely illustrate that for the present systems the XANES peaks can be associated to specific f-orbitals, allowing a direct assignment of spectral features in agreement with the assignment made previously using f-DOS. In O_h symmetry, peak A is mainly affected by the position of a_{2u} while the position of peak C is almost entirely determined the energy of the t_{1u} group of orbitals. Shifting t_{2u} affects mostly peak B and causes a slight shift of peak A. In D_{4h} symmetry, b_{1u} and b_{2u} are very close and determine the intensity of peak A, e_{u2} corresponds to the high-energy shoulder of peak A while e_{u1} and a_{2u} correspond to peak B and C, respectively.

Comparison of CF parameters of 5f orbital splitting with other studies is made difficult by the paucity of works on similar systems. The only previously reported multiplet calculations on the M_4 HERFD XANES on Pb_3UO_6 uranate accounted explicitly for hybridization and found significantly different CF parameters.[32] In our work, the effects of hybridization are not explicitly treated making a direct comparison difficult. The splitting of 5f orbitals from multiplet calculations can be compared with the FDMNES 5f-DOSs (Table S1). The largest discrepancy is found for the a_{2u} (f_{xyz}) orbital of $Cs_2UO_2Cl_4$ predicted at 1.6 eV higher energy by CF calculations. Values for $Cs_2UO_2Cl_4$ can also be compared with energies reported by Vitova et al.,[21] which are very close to the those obtained by FDMNES calculations, and in good agreement with multiplet calculations. A greater mismatch for the a_{2u} (f_{xyz}) orbital is found also in this case. The discrepancy can be ascribed to hybridization effects, which

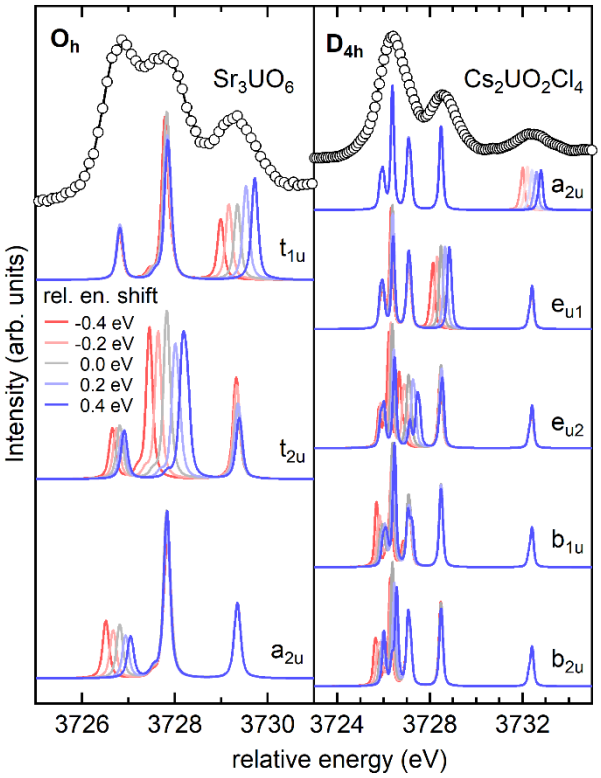

Figure 6: CF XANES calculations obtained by shifting the energy of each group of crystal field-split f-orbitals. Each group of simulation is labelled by the symmetry of the shifted orbitals. Experimental data are shown on top (open circles). The Slater-Condon integrals are reduced to 40% of the atomic value.

are accounted for in DFT and molecular orbital calculations while are not included in our multiplet calculations, where the splitting is entirely induced by the CF. Attempts to include hybridization in our multiplet calculations revealed a strong correlation between CF and hybridization parameters, with the consequent impossibility to determine a unique set of parameters.

Overall, the multiplet calculations allows us to easily identify the nature of the spectral features for the current systems. Despite the CF parameters used in these calculations differ somewhat from the results obtained using FDMNES due to hybridization, we expect that the values reported here would be a good starting point for calculations of U^{5+} and U^{4+} systems where the U local geometry is similar to the samples investigated here.

Conclusions

The present work demonstrates the high sensitivity of M_4 edge HERFD XANES to the U^{6+} local environment. For the first time, a set of M_4 edge HERFD XANES data representative of the variety of U^{6+} local environment, spanning from uranyl to uranate, is shown and analyzed with theoretical calculations. The good agreement of DFT-based XANES calculations with experimental data proves that the spectral differences mainly reflect the different local structure of U^{6+}, with the core-hole effect playing a key role in obtaining the correct energy position and relative intensity of the spectral features. Inspection of the underlying 5f DOS reveals that

the spectral features correspond to specific groups of 5f orbitals. In particular, the main peak at the absorption edge (A) corresponds to non-bonding 5f orbitals while the highest energy peak (C) corresponds to the anti-bonding 5f orbital pointing towards the ligands. This interpretation of spectral features, already accepted for uranyl, is now expanded to a larger class of U local geometries. CFM calculations also show good agreement with experiment and confirms the assignment of peaks to specific 5f orbitals. The splitting of 5f-orbitals determined in the present work may provide a reasonable starting point to investigate U^{5+} and U^{4+} systems with comparable local geometries.

ASSOCIATED CONTENT

Supporting Information

The Supporting Information is available free of charge on the ACS Publications website.

Additional DFT-based calculations (Fig. S1 and S2), schematics of 5f orbital splitting in the three point group considered (Fig. S3), tables reporting the energies of the 5f orbitals obtained by DFT and CF calculations and the Wybourne parameters (Table S1 and S2), example of FDMNES input file (PDF).

Example of Quanty input file generated with the Crispy package (PDF).

AUTHOR INFORMATION

Corresponding Author

* lucia.amidani@esrf.fr, kristina.kvashina@esrf.fr.

Author Contributions

L.A. and K.O.K. developed and designed the study. K.P. synthesized samples. P.M. and K.O.K. performed the experiment. A.V. and L.A. performed CF calculations under the guidance of M.R. L.A. performed DFT-based calculations and wrote the original draft. All authors contributed to the final version of the manuscript.

ACKNOWLEDGMENT

We acknowledge support from the European Research Council (ERC) under grant agreement no. 759696. A.V. and K.O.K. acknowledge support by the Russian Ministry of Science and Education under grant no. 075-15-2019-1891. The authors would like to acknowledge the ESRF for providing beam time.

REFERENCES

(1) K. O. Kvashnina, S. M. Butorin, P. Martin, P. Glatzel, *Phys. Rev. Lett.* **2013**, *111*, 253002.

(2) K. O. Kvashnina, Y. O. Kvashnin, S. M. Butorin, *J. Electron Spectrosc. Relat. Phenom.* **2014**, *194*, 27–36.

(3) K. O. Kvashnina, A. Yu. Romanchuk, I. Pidchenko, L. Amidani, E. Gerber, A. Trigub, A. Rossberg, S. Weiss, K. Popa, O. Walter, R. Caciuffo, A. C. Scheinost, S. M. Butorin, S. N. Kalmykov, *Angew. Chem. Int. Ed.* **2019**, *58*, 17558–17562.

(4) C. Fillaux, J.-C. Berthet, S. D. Conradson, P. Guilbaud, D. Guillaumont, C. Hennig, P. Moisy, J. Roques, E. Simoni, D. K. Shuh, T. Tyliszczak, I. Castro-Rodriguez, C. Den Auwer, *Comptes Rendus Chim.* **2007**, *10*, 859–871.

(5) T. Vitova, I. Pidchenko, D. Fellhauer, T. Pruessmann, S. Bahl, K. Dardenne, T. Yokosawa, B. Schimmelpfennig, M. Altmaier, M. Denecke, J. Rothe, H. Geckeis, *Chem. Commun.* **2018**, *54*, 12824–12827.

(6) T. Vitova, I. Pidchenko, D. Fellhauer, P. S. Bagus, Y. Joly, T. Pruessmann, S. Bahl, E. Gonzalez-Robles, J. Rothe, M. Altmaier, M. A. Denecke, H. Geckeis, *Nat. Commun.* **2017**, *8*, 16053.

(7) G. Leinders, R. Bes, J. Pakarinen, K. Kvashnina, M. Verwerft, *Inorg. Chem.* **2017**, *56*, 6784–6787.

(8) E. Gerber, A. Yu. Romanchuk, I. Pidchenko, L. Amidani, A. Rossberg, C. Hennig, G. B. M. Vaughan, A. Trigub, T. Egorova, S. Bauters, T. Plakhova, M. O. J. Y. Hunault, S. Weiss, S. M. Butorin, A. C. Scheinost, S. N. Kalmykov, K. O. Kvashnina, *Nanoscale* **2020**, 17951–18480.

(9) M. O. J. Y. Hunault, G. Lelong, L. Cormier, L. Galoisy, P.-L. Solari, G. Calas, *Inorg. Chem.* **2019**, *58*, 6858–6865.

(10) C. H. Booth, Y. Jiang, D. L. Wang, J. N. Mitchell, P. H. Tobash, E. D. Bauer, M. A. Wall, P. G. Allen, D. Sokaras, D. Nordlund, T.-C. Weng, M. A. Torrez, J. L. Sarrao, *Proc. Natl. Acad. Sci.* **2012**, *109*, 10205–10209.

(11) J. G. Tobin, S. Nowak, C. H. Booth, E. D. Bauer, S.-W. Yu, R. Alonso-Mori, T. Kroll, D. Nordlund, T.-C. Weng, D. Sokaras, *J. Electron Spectrosc. Relat. Phenom.* **2019**, *232*, 100–104.

(12) M. Zegke, X. Zhang, I. Pidchenko, J. A. Hlina, R. M. Lord, J. Purkis, G. S. Nichol, N. Magnani, G. Schreckenbach, T. Vitova, J. B. Love, P. L. Arnold, *Chem. Sci.* **2019**, *10*, 9740–9751.

(13) S. T. Liddle, *Angew. Chem. Int. Ed.* **2015**, *54*, 8604–8641.

(14) P. C. Burns, *Can. Mineral.* **2005**, *43*, 1839–1894.

(15) S. M. Butorin, K. O. Kvashnina, J. R. Vegelius, D. Meyer, D. K. Shuh, *Proc. Natl. Acad. Sci.* **2016**, *113*, 8093–8097.

(16) S. M. Butorin, *Inorg. Chem.* **n.d.**, 14.

(17) H. Ramanantoanina, G. Kuri, C. Daul, J. Bertsch, *Phys. Chem. Chem. Phys.* **2016**, *18*, 19020–19031.

(18) D.-C. Sergentu, T. J. Duignan, J. Autschbach, *J. Phys. Chem. Lett.* **2018**, *9*, 5583–5591.

(19) M. Diaz-Lopez, S. A. Guda, Y. Joly, *J. Phys. Chem. A* **2020**, *124*, 6111–6118.

(20) D. B. Prieur, K. Popa, J.-F. Vigier, A. C. Scheinost, P. M. Martin, *J. Nucl. Mater.* **2019**, *516*, 303–308.

(21) T. Vitova, J. C. Green, R. G. Denning, M. Löble, K. Kvashnina, J. J. Kas, K. Jorissen, J. J. Rehr, T. Malcherek, M. A. Denecke, *Inorg. Chem.* **2015**, *54*, 174–182.

(22) P. Glatzel, A. Harris, P. Marion, M. Sikora, T.-C. Weng, C. Guilloud, S. Lafuerza, M. Rovezzi, B. Detlefs, L. Ducotté, *J. Synchrotron Radiat.* **2021**, *28*, 362–371.

(23) O. Bunău, Y. Joly, *J. Phys. Condens. Matter* **2009**, *21*, 345501.

(24) O. Bunău, Y. Joly, *Phys. Rev. B* **2012**, *85*, 155121.

(25) G. Bergerhoff, I. Brown, F. Allen, others, **1987**.

(26) M. W. Haverkort, G. Sangiovanni, P. Hansmann, A. Toschi, Y. Lu, S. Macke, *EPL Europhys. Lett.* **2014**, *108*, 57004.

(27) M. Retegan, *Crispy: V0.7.2*, **2019**.

(28) J. Qiu, P. C. Burns, *Chem. Rev.* **2013**, *113*, 1097–1120.

(29) R. B. King, *Chem. Mater.* **2002**, *14*, 3628–3635.

(30) M. O. J. Y. Hunault, D. Menut, O. Tougait, *Crystals* **2021**, *11*, 56.

(31) T. Vitova, I. Pidchenko, S. Biswas, G. Beridze, P. W. Dunne, D. Schild, Z. Wang, P. M. Kowalski, R. J. Baker, *Inorg. Chem.* **2018**, *57*, 1735–1743.

(32) S. M. Butorin, K. O. Kvashnina, A. L. Smith, K. Popa, P. M. Martin, *Chem. - Eur. J.* **2016**, *22*, 9693–9698.

(33) L. Amidani, G. B. M. Vaughan, T. V. Plakhova, A. Yu. Romanchuk, E. Gerber, R. Svetogorov, S. Weiss, Y. Joly, S. N. Kalmykov, K. O. Kvashnina, *Chem. – Eur. J.* **2021**, *27*, 252–263.

(34) B. N. Figgis, M. A. Hitchman, *Ligand Field Theory and Its Applications*, Wiley-VCH, **2000**.

(35) R. G. Denning, *J. Phys. Chem. A* **2007**, *111*, 4125–4143.

(36) *Unpublished Data*, **n.d.**

(37) J. Kolorenč, K. O. Kvashnina, *MRS Adv.* **2018**, *3*, 3143–3148.

(38) F. de Groot, *Coord. Chem. Rev.* **2005**, *249*, 31–63.

(39) S. Agrestini, C.-Y. Kuo, M. Moretti Sala, Z. Hu, D. Kasinathan, K.-T. Ko, P. Glatzel, M. Rossi, J.-D. Cafun, K. O. Kvashnina, A. Matsumoto, T. Takayama, H. Takagi, L. H. Tjeng, M. W. Haverkort, *Phys. Rev. B* **2017**, *95*, 205123.

(40) A. Amorese, M. Sundermann, B. Leedahl, A. Marino, D. Takegami, H. Gretarsson, A. Gloskovskii, C. Schlueter, M. W. Haverkort, Y. Huang, M. Szlawska, D. Kaczorowski, S. Ran, M. B. Maple, E. D. Bauer, A. Leithe-Jasper, P. Hansmann, P. Thalmeier, L. H. Tjeng, A. Severing, *Proc. Natl. Acad. Sci.* **2020**, *117*, 30220–30227.

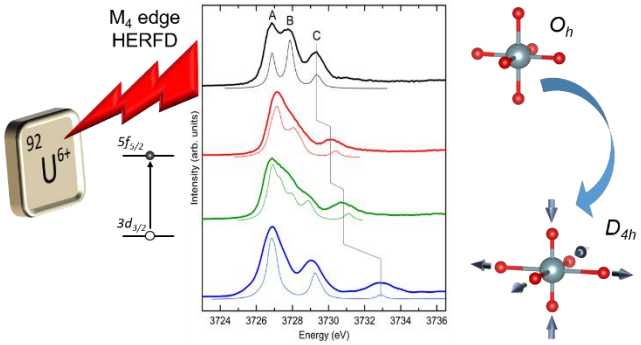

Insert Table of Contents artwork here